Analysis of a Split-Flow Inertial Particle Separator by Finite Elements

D. S. Breitman,* E. G. Dueck,† and W. G. Habashi‡
Pratt & Whitney Canada, Ontario, Canada

This paper presents an analytical design method for inertial particle separators required for aviation gas turbines applications to helicopters. The solution of the flowfield inside the separator is based on a finite element code for the radial equilibrium equation. The aerodynamic forces calculated are then used to predict the trajectories of solid particles of various sizes. Several separator designs are demonstrated and a very efficient final configuration is determined.

Nomenclature

A_p = particle cross-sectional area
b = blockage factor
C_D = drag coefficient
C_r, C_z, C_θ = absolute velocity in r, z, and θ directions, respectively
d = diameter of maximum cross-sectional area of particle
E_N, E_T = normal and tangential restitution coefficients, respectively
F_B = buoyancy force
$F_{Dr}, F_{Dz}, F_{D\theta}$ = drag force in r, z, and θ directions, respectively
g = gravitational force
I = rothalpy, (total enthalpy $-\Omega r V_\theta$)
K = global influence matrix
k = element influence matrix
L = Laplacian operator
M = Mach number
m = particle mass
$\dot{m}$ = duct mass flow rate
N = finite element shape function
Re = Reynolds number
R = governing equation's residual, $= [K]\{\psi\} - \{\omega\}$
r = radial coordinate
S = entropy
s = particle shape factor
T = temperature
V' = particle relative velocity, particle velocity − flow velocity
V_θ = relative velocity in θ direction, $C_\theta - \Omega r$
V'_{N_1}, V'_{N_2} = particle normal velocity before and after impact, respectively
V'_{T_1}, V'_{T_2} = particle tangential velocity before and after impact, respectively
Z = axial coordinate
α = under-/over-relaxation parameter
β_1 = particle incidence angle
$\delta\Psi$ = change in stream function during one iteration
(ξ, η) = local undistorted coordinates within element
η_ω = sand separation efficiency by weight
θ = circumferential coordinate
ρ = density of air
ϕ = inclination of engine axis to horizontal
ψ = stream function
ω = vorticity
Ω = angular velocity
[ ] = matrix
{ } = vector

Subscripts

i,j = nodal quantity

Introduction

HELICOPTERS, especially military ones, make numerous takeoffs and landings from unprepared areas where they are exposed to ingestion of large amounts of sand and dust. This causes erosion of engine components, appreciably reducing the engine's life expectancy. Early efforts to protect the engine involved the use of filters located in the engine inlet. These filters provide excellent separation, are lightweight, and have a low initial cost. However, periodic cleaning and replacement is necessary to maintain tolerable pressure losses.

These considerations encouraged development of inertial particle separators which can be wholly integrated with the engine, are self-cleaning, and have a fixed pressure drop. To create a large inertia field for exceptional separation, swirl vanes have to be employed in the inlet. The inclusion of swirl induces high performance penalties, and the vanes require deicing.

Thus, simplicity, performance, and ruggedness are compelling reasons to develop a swirl-free, low-loss inertial-type particle separator which still provides effective engine

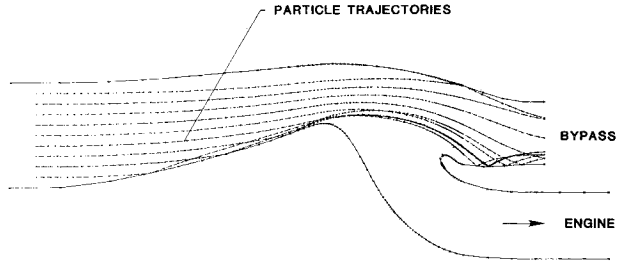

Fig. 1 Ideal operation of an inertial particle separator with small (light) particles.

Received Dec. 12, 1983; revision received Sept. 24, 1984.

*Senior Aerodynamicist.
†Chief, Turbofan Compressor Aerodynamics.
‡Consultant; also, Professor, Concordia University, Montreal, Canada.

protection. In this concept the entering airflow is turned sharply inward to the engine centerline. The larger inertia of the sand and dust propels them to the outer periphery where they are collected and dumped overboard, as illustrated in Fig. 1. Larger particles, which do not follow the airflow streamline, hit the inner hub wall, which is angled to deflect the particles toward the outer periphery and, hence, out the bypass, Fig. 2.

Analysis

The analysis objective for a specific design concept is to predict the separation efficiency for a given sand distribution. This requires trajectory prediction for various particle sizes as they are acted upon by the separator aerodynamic forces. In turn, this requires an aerodynamic flowfield solution inside the separator.

The analytical model presented here consists of two main codes: flowfield computation by a finite element through-flow program and trajectory analysis by a particle trajectory program.

Flowfield Numerical Computation

Governing Equations and Boundary Conditions

The flow is governed by the radial equilibrium equation[1,2]:

$$C_Z\left(\frac{\partial C_z}{\partial r}-\frac{\partial C_r}{\partial z}\right)=-\left(\frac{V_\theta}{r}\frac{\partial(rC_\theta)}{\partial r}+\frac{T\partial S}{\partial r}-\frac{\partial I}{\partial r}\right) \tag{1}$$

By defining

$$C_z=\frac{\dot m}{2\pi\rho rb}\frac{\partial\Psi}{\partial r} \tag{2}$$

$$C_r=-\frac{\dot m}{2\pi\rho rb}\frac{\partial\Psi}{\partial z} \tag{3}$$

Eq. (1) can be rewritten as

$$\frac{\partial}{\partial r}\left(\frac{1}{\rho rb}\frac{\partial\Psi}{\partial r}\right)+\frac{\partial}{\partial z}\left(\frac{1}{\rho rb}\frac{\partial\Psi}{\partial z}\right)=-\frac{2\pi}{\dot mC_z}\left(\frac{V_\theta}{r}\frac{\partial(rC_\theta)}{\partial r}+\frac{T\partial S}{\partial r}-\frac{\partial I}{\partial r}\right) \tag{4}$$

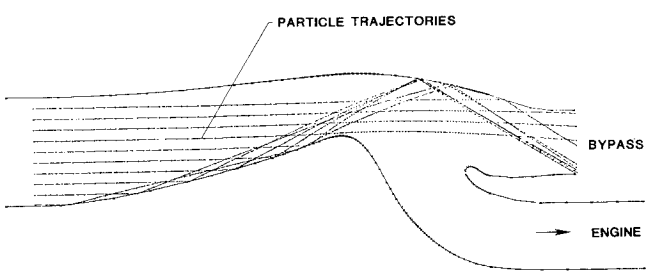

Fig. 2 Ideal operation of an inertial particle separator with large (heavy) particles.

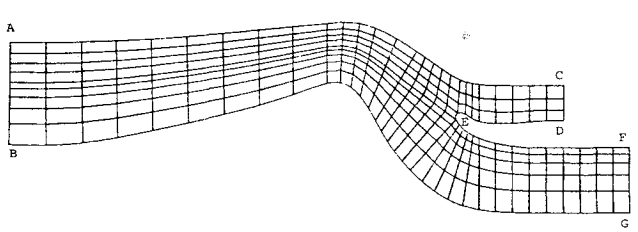

Fig. 3 Finite element discretization.

where the boundary conditions are (see Fig. 3):

Hub	BG:	$\Psi=0$
Shroud	AC:	$\Psi=1$
Separator	DEF:	$\Psi=\Psi_0$; a constant determined by bypass ratio
Inlet	AB:	$\frac{\partial\Psi}{\partial n}=0$
Exit	CD,FG:	$\frac{\partial\Psi}{\partial n}=0$ (5)

where n is the outward normal to the surface.

Finite Element Discretization and Solution Procedure

Curvilinear eight-node isoparametric elements are used where both the function Ψ and geometry have parabolic representation. In each element

$$\Psi=\sum_{i=1}^{8}N_i(\xi,\eta)\Psi_i;\quad z=\sum_{i=1}^{8}N_i(\xi,\eta)z_i;\quad r=\sum_{i=1}^{8}N_i(\xi,\eta)r_i \tag{6}$$

N_i being the parabolic shape functions written in terms of the local undistorted element coordinates ξ and η.

Applying the Galerkin-weighted residual method to Eq. (4) results in the matrix equation

$$[K]\{\Psi\}=\{\omega\} \tag{7}$$

where

$$k_{ij}=\int\!\!\int\frac{1}{\rho rb}\left(\frac{\partial N_i}{\partial r}\frac{\partial N_j}{\partial r}+\frac{\partial N_i}{\partial z}\frac{\partial N_j}{\partial z}\right)drdz \tag{8}$$

$$\omega_i=\int\!\!\int\frac{2\pi N_i}{\dot mC_z}\left(\frac{V_\theta}{r}\frac{\partial(rC_\theta)}{\partial r}+\frac{T\partial S}{\partial r}-\frac{\partial I}{\partial r}\right)drdz \tag{9}$$

The numerical integration of Eqs. (8) and (9) is carried out using a 3×3 Gaussian integration procedure.

The mesh generation of the current split flow is totally automated and an illustrative grid is shown in Fig. 3. The nonlinear algebraic system of equations represented by Eq. (7) is recast in the form:

$$[K']^n\{\delta\psi\}^{n+1}=-\alpha\{R\} \tag{10}$$

where K' is a symmetric, banded, matrix operator approximating the physics of the flow, $[K]$, normally taken as the Laplacian operator scaled by the "nodal" densities, i.e., $[L]/\{\rho_i\}$. Matrix $[K']$ is decomposed at the first iteration by the Cholesky decomposition and only the backward substitution step is needed at each iteration for the solution of Eq. (10). All results shown in the paper are carried out to an $L-2$ residual for R of less than 10^{-5}, where

$$R_{L-2}=\sum_{\text{nodes}}R_i^2\le10^{-5} \tag{11}$$

Typically, a solution requires 5 to 6 iterations and takes approximately 20 s of CPU time on a CDC Cyber 175.

Particle Trajectories

Governing Equations

The particle motion within a given flowfield is determined by a resolution of forces. These include the aerodynamic

drag, buoyancy, gravity, and kinematic forces. The buoyancy and gravitational forces are normally assumed to be negligible. Written in cylindrical polar coordinates, the equations of motion are

$$m\ddot{z}+F_{Dz}-(mg-F_B)\sin\phi=0 \quad (12)$$

$$m\ddot{r}+F_{Dr}-mr\dot{\theta}^2+(mg\cos\phi)\sin\theta-(F_B\cos\phi)\sin\theta=0 \quad (13)$$

$$2m\dot{r}\dot{\theta}+mr\ddot{\theta}+F_{D\theta}+(mg\cos\phi)\cos\theta-(F_B\cos\phi)\cos\theta=0 \quad (14)$$

where r, θ, and z define the particle location. The corresponding drag forces, F_{Dr}, $F_{D\theta}$, and F_{Dz}, are assumed positive if the particle velocity in these directions is greater than the air velocity. The angle ϕ gives the inclination of engine axis z from the horizontal. F_B is the buoyancy force. The complete force diagram is shown in Fig. 4.

Aerodynamic Drag

The particle drag forces, in terms of a drag coefficient C_D, are

$$F_D=C_D\tfrac{1}{2}(\rho/g)V'A_p \quad (15)$$

Many empirical formulations for the drag coefficient of a spherical particle have been derived from experimental data. The formulations, in the form of a correction to Stokes' drag law, are valid for Reynolds numbers corresponding to the entire flow region. The following is used in the present analysis[3]:

$$C_D=\frac{24}{Re}\frac{(1+0.15Re^{0.687})\,[1+e^{-(0.427/M^{4.63})-(3.0/Re^{0.88})}]}{1+(M/Re)(3.82+1.28e^{-1.25Re/M})} \quad (16)$$

Typical ranges in the separator are between 0.001 and 0.2 for Mach number and 0.1 to 10.0 for Reynolds number.

Shape Factor

Equation (16) has been derived for spherically shaped particles. Irregular shaped, nonspherical particles will, for an equivalent cross-sectional area, as in a flat plate, result in a drag equivalent to that of the sphere but with a lower particle mass. The larger mass of the spherical model gives a particle excess momentum resulting in overprediction of the separation efficiency. General Electric[4] recognized this and empirically derived a "shape factor" based on test results from their R&D program. This shape factor is

$$s=\text{true volume of particle}/d^3 \quad (17)$$

where d is the diameter of the maximum cross-sectional area.

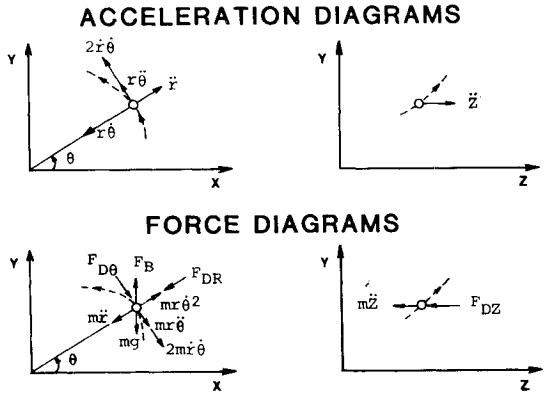

Fig. 4 Acceleration and force diagrams.

For an exact sphere, $s=\pi/6$. A shape factor of 0.26-0.28 was recommended for random particles.[4] A shape factor of $0.2618(\pi/12)$ is used in the present analysis. This number was derived from a trial-and-error matching of the code prediction with experimental results.

Bounce Characteristics

The collision/reflection of a particle from a hard duct wall is, to some extent, a random process because of the irregular shape of the particle. Considerable effort[5-7] has been expended in deriving empirical expressions to model the collision/reflection of typical sand particles. The following expressions[8,9] predict reflected normal and tangential velocities as functions of impingement angle (β_1) and impingement normal and tangential velocities (V_N; V_T).

$$E_T=V'_{T_2}/V'_{T_1}=1.0-2.12\beta_1+3.0775\beta_1^2-1.1\beta_1^3 \quad (18)$$

$$E_N=V'_{N_2}/V'_{N_1}=1.0-0.4159\beta_1-0.4994\beta_1^2+0.292\beta_1^3 \quad (19)$$

Recently acquired test data revealed a discrepancy with analysis for large particle sizes, where bounce is the predominant separating mechanism. The much simpler empirical expressions for restitution coefficients provide better agreement with test results and are incorporated into the analysis:

$$E_T=V'_{T_2}/V'_{T_1}=1.0 \quad (20)$$

$$E_N=V'_{N_2}/V'_{N_1}=0.85 \quad (21)$$

Two sample trajectory plots are presented. Figure 5 shows the trajectory plots for 5-μm particles. Of particular interest is that the code shows some of the particles actually being carried back around the splitter into the core; a result of the stagnation point falling on top of the splitter.

Figure 6 shows the trajectory plots for 100-μm particles. Here, where the particle mass, and, therefore, momentum, is much larger, a separation efficiency of 100% is predicted.

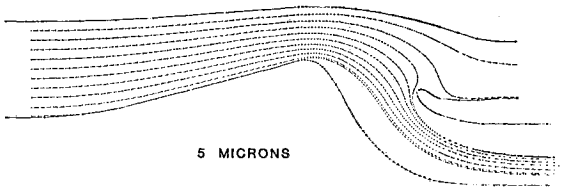

Fig. 5 Particle trajectory plot, 5 μm.

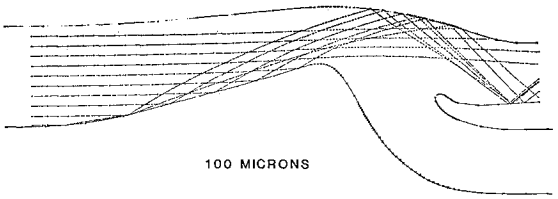

Fig. 6 Particle trajectory plot, 100 μm.

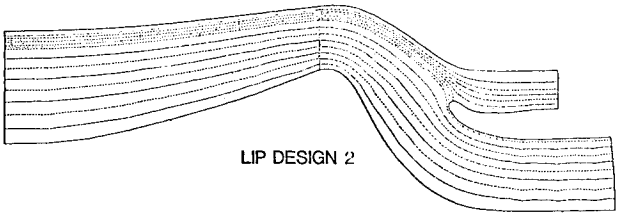

Fig. 7 Finite element program streamline prediction; lip design 2.

General Description of Design

An axisymmetric inertial separator is designed such that the entering airflow is turned sharply inward to the engine centerline. The larger inertia of sand and dust propels them to the outer periphery where they are collected and dumped overboard. Large particles, which do not follow the airflow streamlines, hit the inner hub wall, which is angled to deflect the particles toward the outer periphery and, hence, out the bypass.

Use of Finite Element Through-Flow Analysis Code

This rather unique geometry results in an unusual intake to the engine core. Because of the splitter proximity and low bypass ratio, there is a high positive splitter incidence inducing the stagnation point to fall on top of the lip. As the flow reverses and follows the sharp turn of the splitter lip, it undergoes rapid acceleration followed by abrupt deceleration. This may cause the flow to stall along the underside of the splitter lip as it enters the core duct. With the aid of the finite element through-flow analysis program, several splitter lip designs were investigated with the objective to design a splitter with correct leading-edge incidence. Streamline curvature routines or programs requiring separate treatment of (or iterative treatment between) core and bypass are not able to model this region correctly.[9,10] The unique capability of this finite element method (FEM) program to model this region correctly and consistently in one pass lends immeasurably to the predictive capability of the total scheme.

Three splitter lip designs were selected for testing. Figure 7 shows a typical FEM streamline prediction. Figure 8 shows the predicted splitter lip Mach number along the lower surface of each design.

Lip 1 is simply a $\sqrt{2}$:1 flat ellipse. If the stagnation point were to fall on the leading edge of the ellipse, the flow would experience constantly decreasing radii of curvature as it negotiated the turn into the core duct. However, since the stagnation point is off center, the flow will experience a large acceleration back as it passes over the peak curvature, combined with area convergence as flow is drawn into the engine core, resulting in very high velocities throughout the turn. This may cause the flow to separate on the underside of the splitter lip as the flow diffuses from this Mach number peak.

Lip 2 is a 2:1 ellipse inclined at an angle of 47 deg to have the stagnation point fall on the leading edge of the ellipse. Thus diffusion along the lower side is greatly reduced in comparison to design 1. Note that the leading edge of the ellipse is not the foremost axial location of the splitter.

Lip 3 is a 2:1 ellipse inclined at an angle of 80 deg and extended 0.30 in. further upstream than lip 2. With this increased inclination, as the lip is moved upstream, the stagnation point can still be induced to fall on the lip leading edge. The higher Mach numbers are due in part to the smaller flow cross-sectional area into the core duct. The purpose of this option is to further improve the separator "step/gap" ratio, hence, improve particle separation efficiency while exacting a small compromise on inlet pressure recovery.

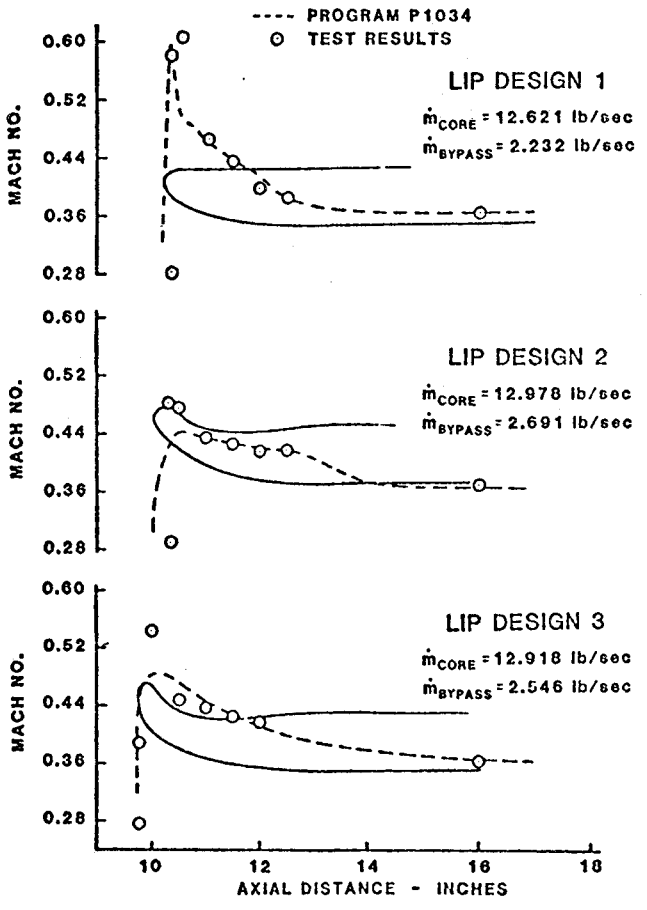

Fig. 8 Splitter lip Mach number—lower side.

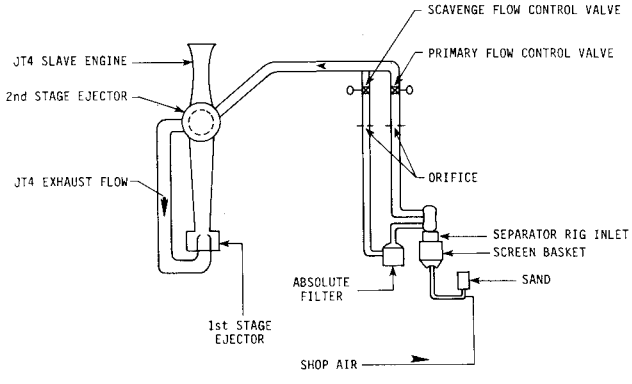

Fig. 9 Schematic of test rig.

Test Program

Testing of the particle separator was conducted at the Pratt & Whitney Research and Development Center located in West Palm Beach, Fla. A JT4 slave engine was used as an ejector to provide the necessary suction for primary and scavenge flow lines. Figure 9 shows a schematic of the test setup.

Aerodynamic Performance Tests

The performance test procedure consisted largely of two tasks: establishing the desired flow conditions and recording the necessary aerodynamic data. The primary and scavenge airflows were regulated by control valves positioned downstream of the test section and filters. Instrumented orifice plates were used to monitor the airflows. This arrangement facilitated the setting of each aerodynamic performance test point.

The separator hardware was extensively instrumented to evaluate the aerodynamic performance and study the flow behavior in critical areas. A total of 119 channels were recorded for each performance data point. Scani-valves and transducers were used to read the aerodynamic data of which a hard copy was immediately obtained from an on-line computer.

Sand Ingestion Tests

Sand ingestion tests were conducted using a variety of sand types and mixtures. In particular, two sand types were extensively used: military C-spec sand comprised of 0-1000-μm particles, and AC coarse test dust, comprised of 0-200-μm particles.

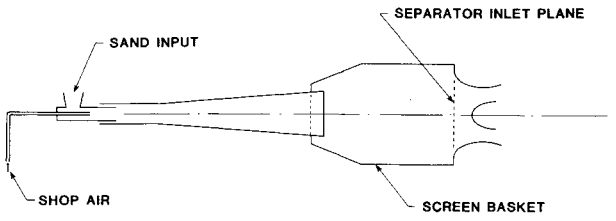

Fig. 10 Sand injection system for particle separator testing.

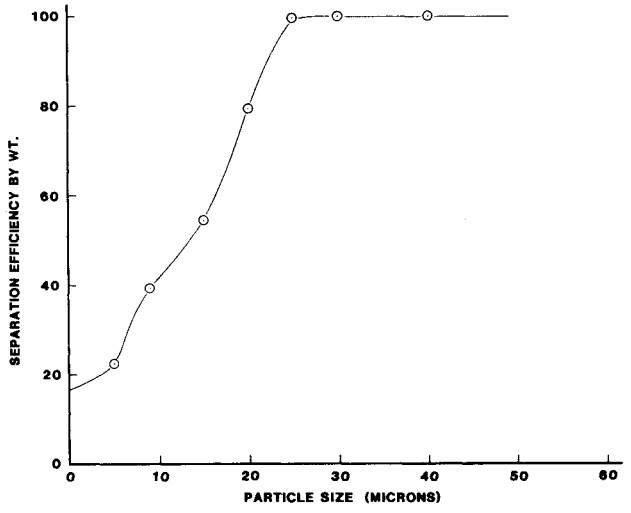

Fig. 11 Predicted separation efficiencies (20% bypass ratio).

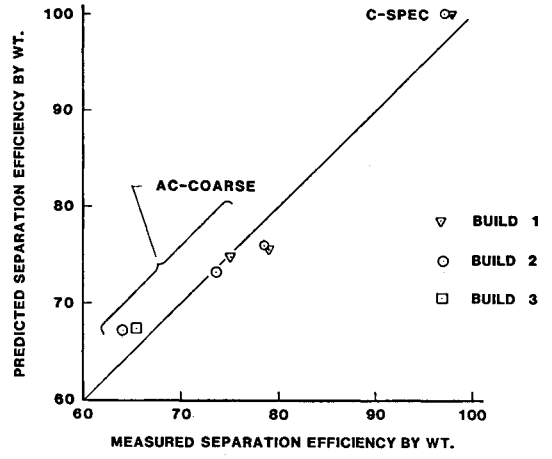

Fig. 12 Comparison between predicted and measured efficiencies.

The sand injection setup consists of an ejector duct system powered by shop air and a fine-mesh basket fixed to the separator inlet bellmouth. Sand is introduced manually via a hopper at the inlet of the ejector. From the hopper the sand travels down a diffuser nozzle which dumps into the screen basket. The basket is constructed from type 304 stainless steel, twilled dutch weave filter cloth with a 75-μm opening, spot welded to the inside of a lightweave frame made of a 3/8-in.-diam solid rod. The sand migrates approximately 3 ft inside the basket to the separator inlet. Any sand that does not enter the separator inlet is trapped inside the basket. Figure 10 shows a schematic of the sand injection system.

Only the bypass airflow is filtered. This is accomplished by using two Donaldson EBA 15-0003 paper filter elements in parallel. Before each sand injection test the filter elements are cleaned and weighed and a known amount of sand is placed at the hopper. After each test, the filters are weighed again, and the inlet basket inspected for any residual sand. The weight of the residual sand is subtracted from the input sand weight and the separation efficiency is computed as

$$\eta_w = \frac{\text{weight of sand collected in filters}}{\text{weight of sand entering separator inlet}}$$

Any sand that cannot be accounted for is assumed to end up in the core flow, thus the actual separation efficiency cannot be less than the computed efficiency.

Results and Comments

Figure 8 gives a comparison of predicted and measured splitter lip Mach numbers. The discrepancy in the prediction of the peak Mach numbers for lips 2 and 3 can be attributed to viscous flow effects since stall is observed in the area of large diffusion along the shroud just past the hub apex. Since our finite element code is inviscid, the large separation zone located on the shroud must be simulated by using a displaced geometry. Any inaccuracy in the modeling of this stalled region would, of course, lead to inaccurate predictions. This displaced geometry was defined by an inverse integral boundary-layer routine and correlated with experimental test measurements. This, and follow-on work, will be reported in the future. In spite of this shortcoming, the analysis is successful in that both lips 2 and 3 demonstrate better than a 10% improvement in aerodynamic performance (i.e., engine inlet total pressure drop) over lip 1.

To predict separation efficiency for a sand mixture, the analysis must be performed for the complete range of particle sizes in the sand mixture. The individual efficiencies are then integrated for the size distribution of a specified mixture. Figure 11 shows the predicted separation efficiencies correlated with particle size for one of the configuration tests.

Fine dust or other particles follow the flowfield until they negotiate the sharp downward turn toward the engine core. When exposed to the inertial field created by the turn, the particle's momentum causes its path to diverge from the flow and, hence, on toward the bypass duct. For extremely fine particles (<10 μm diameter) the inertial forces are small relative to drag forces, resulting in the particle following the flowfield into the engine core.

For larger particles the aerodynamic drag force is small compared to the inertia forces, resulting in the particle trajectory being almost independent of the flowfield. These particles collide with the duct walls which are designed to direct the particles into the bypass duct. As can be seen in Fig. 11 for particles greater than 25 μm, the separation efficiency is predicted to be 100%.

Figure 12 compares predicted efficiencies with test results from our test program. Good agreement exists between the theory and test results. In the past, modeling of a particle separator could only serve as a starting point, with hardware testing providing actual sand separation efficiencies. Although bench testing will always be a necessary part of any development program, with the recent advances in numerical methods, theoretical predictions are becoming increasingly more accurate and reliable.

Acknowledgments

The authors wish to acknowledge the technical assistance of Messrs. R. A. Thompson and S. Zuquim of Pratt & Whitney, Canada, and W. Haynie of Pratt & Whitney, Florida.

References

[1] Habashi, W. G., "Numerical Methods of Turbomachinery," *Recent Advances in Numerical Methods in Fluids*, Vol. 1, edited by C. Taylor and K. Morgan, Pineridge Press, U.K., 1980, Chap. 8, pp. 241-282.

[2]Habashi, W. G. and Youngson, G. G., "A Transonic Quasi-3D Analysis for Gas Turbine Engines Including Split-Flow Capability for Turbofans," *International Journal for Numerical Methods in Fluids*, Vol. 3, No. 1, 1983, pp. 1-22.

[3]Carlson, D. J. and Hoglund, R. F., "Particle Drag and Heat Transfer in Rocket Nozzles," *AIAA Journal*, Vol. 2, Nov. 1964, pp. 1980-1984.

[4]Duffy, R. J. et al., "Integral Engine Inlet Particle Separator," *Design Guide*, Vol. II, USAAMRDL-TR-75-31B, Aug. 1975.

[5]Wakeman, T. and Tabakoff, W., "Measured Particle Rebound Characteristics Useful for Erosion Prediction," ASME Paper 82-GT-170, 1982.

[6]Grant, G. and Tabakoff, W., "Erosion Prediction in Turbomachinery Resulting from Environmental Solid Particles," *Journal of Aircraft*, Vol. 12, May 1975, pp. 471-478.

[7]Beacher, B., Tabakoff, W., and Hamed, A., "Improved Particle Trajectory Calculations Through Turbomachinery Affected by Coal Ash Particles," *Journal of Engineering for Power*, Vol. 104, Jan. 1982, pp. 64-76.

[8]Tabakoff, W. and Hamed, A., "Aerodynamic Effects on Erosion in Turbomachinery," *Proceedings of the 1977 Joint Gas Turbine Congress*, Tokyo, May 1977, pp. 574-581.

[9]Hamed, A., "Particle Dynamics of Inlet Flowfields with Swirling Vanes," *Journal of Aircraft*, Vol. 19, Sept. 1982, pp. 707-712.

[10]Fabian, J. M. and Oates, G. G., "Analysis of Flows within Particle Separators," ASME Paper 77-WA/FE-21, 1977.